Potential Dependent Structure and Stability of Cu(111) in Neutral Phosphate Electrolyte

Yvonne Grunder [1], **Jack Beane** [1], **Adam Kolodziej** [2], **Christopher A. Lucas** [1] and **Paramaconi Rodriguez** [2,*]

[1] Department of Physics, University of Liverpool, Liverpool L69 7ZE, UK;
Yvonne.Grunder@liverpool.ac.uk (Y.G.); sgjbeane@student.liverpool.ac.uk (J.B.);
clucas@liverpool.ac.uk (C.A.L.)

[2] School of Chemistry, University of Birmingham. Birmingham B15 2TT, UK; AXK595@student.bham.ac.uk

[*] Correspondence: p.b.rodriguez@bham.ac.uk

Abstract: Copper and copper oxide electrode surfaces are suitable for the electrochemical reduction of CO_2 and produce a range of products, with the product selectivity being strongly influenced by the surface structure of the copper electrode. In this paper, we present in-situ surface X-ray diffraction studies on Cu(111) electrodes in neutral phosphate buffered electrolyte solution. The underlying mechanism of the phosphate adsorption and deprotonation of the (di)-hydrogen phosphate is accompanied by a roughening of the copper surface. A change in morphology of the copper surface induced by a roughening process caused by the formation of a mixed copper–oxygen layer could also be observed. The stability of the Cu(111) surface and the change of morphology upon potential cycling strongly depends on the preparation method and history of the electrode. The presence of copper islands on the surface of the Cu(111) electrode leads to irreversible changes in surface morphology via a 3D Cu growth mechanism.

Keywords: Cu(111); electrochemical interface; in-situ X-ray diffraction

1. Introduction

Compared to many metal catalysts, copper surfaces have been proven to electrochemically convert CO_2 to high value and energy-dense products, such as methane ethylene, formic acid, methanol and ethanol amongst others. However, the efficiency and the selectivity are far from optimal and the parameters controlling these factors are not-fully understood. Differences in reactivity and selectivity have been variously ascribed to surface area, particle size, surface structure and roughness and the electrolyte composition [1–6]. More recently, the effect of the role of the oxygen content of the copper catalyst and the oxidation state of the copper on the electrocatalytic activity and selectivity have illustrated the high complexity of the system. Oxide-derived Cu catalysts have shown high-selectivity towards the formation of C_2 products [7–10]. Such selectivity has been attributed to changes in the surface structure, including roughness and defects, with active sites being generated during the reduction pretreatment of the Cu-oxide catalyst. However, more recently, in addition to the structural factors, the presence of Cu^+ and residual subsurface oxygen has been suggested to affect the product selectivity [5,11,12]. Mistry et al. demonstrated, via operando XAFS, the presence of Cu^+ species and subsurface oxygen during the carbon dioxide reduction reaction [5]. In another report, LeDuff et al. [7] implemented a pulse sequence between reduction potentials where the carbon dioxide reduction reaction (CO2RR) takes place (< -0.5 V) and a potential in the region between -0.2 and -0.35 V vs. RHE where the co-adsorption of OH and other anions takes place [13]. They concluded that the positive potential of the pulse has a significant effect in the catalytic activity and selectivity of the copper

single-crystal electrodes towards the CO2RR. This was associated to the adsorbed species, presumably OH or anions, at the surface of the Cu single crystal electrodes which prevent any irreversible damage or changes to the Cu surface structure [7].

In this paper, we present the in-situ characterization by surface X-ray diffraction of the Cu(111) electrode at positive potentials with the aim to determine the composition and structure of the electrochemical interface. The key to understanding the stability and reactivity of the Cu(111) electrode is to control the surface morphology during the preparation of the clean surface. Depending on the details of surface preparation, two different Cu(111) surfaces can be obtained; although macroscopically rather rough, one surface is completely stable during potential cycling that involves considerable modification of the surface structure. The other surface gives rise to X-ray scattering features consistent with the presence of twinned Cu nano-islands and, although this surface exhibits a similar potential-dependent restructuring, it is not stable during potential cycling. The direct correlation of structural stability, only available via in-situ structural characterization, and reactivity is vital to understanding structure–reactivity relationships, especially in studies of more active metal electrodes [14,15].

2. Materials and Methods

The Cu(111) single crystal working electrode (MaTeck, miscut < 0.1°) was prepared by electropolishing for 10 s in 70 % orthophosphoric acid at 2 V against a high-surface area copper mesh. The crystal was then rinsed in ultra-pure water, covered with the electrolyte solution and transferred to the electrochemical cell. A copper wire was used as counter electrode and an Ag/AgCl electrode was used for the reference electrode. All potentials are quoted against this reference electrode. The experimental procedure for the surface X-ray diffraction experiments followed that of similar studies reported previously [16,17]. Surface X-ray diffraction measurements were carried out on the I07 beamline at Diamond Light Source (Harwell Science and Innovation Campus, Fermi Ave, Didcot OX11 0DE, Oxford, UK) [18], with a monochromatic beam of 25 keV X-rays. Beam defining slits were 0.5 mm × 0.5 mm and the beam size at the sample was estimated to be 200 μm × 300 μm (vertical × horizontal). The sample was mounted on a (2 + 3) circle diffractometer [19]. A 2D Pilatus Dectris 1 M detector (DECTRIS Ltd., Baden-Daettwil, Switzerland) was used for the data acquisition. For the measurement of crystal truncation rods, scans along the Q_z (surface normal) direction at specific points in reciprocal space were recorded. Background correction and standard instrumental corrections were applied to the dataset to be able to model the intensity distribution [20,21]. Errors on the individual data points were a combination of the statistical error and an estimated 10% systematic error. The model of X-ray diffraction was obtained using a Python (Python Software Foundation, Beaverton, OR, USA) program and the integrated lmfit leastsquare fitting routine, which returned the best values for the relaxation, coverage and β-factor. The Cu(111) surface has a close packed structure with a hexagonal unit cell, where the surface normal is along the $(0,0,L)_{hex}$ direction and the surface plane contains the $(H,0,0)_{hex}$ and $(0,K,0)_{hex}$ vectors, which are separated by 60°. The Miller indices H, K, and L have units of $a^* = b^* = 4\pi/\sqrt{3}a_{NN}$ and $c^* = 2\pi/\sqrt{6}a_{NN}$, where the nearest neighbour for copper is $a_{NN} = 2.556$ Å.

3. Results

The Cu(111) surfaces were characterised in a phosphate buffered electrolyte by surface X-ray diffraction and with electrochemical methods.

3.1. Electrochemical Characterization

The Cu(111) electrode was characterised in phosphate buffer solution of concentration equal to 0.01 M, 0.05 M and 0.1 M at different pH values of 6 and 8 with cyclic voltammetry at different scan rates (Figure 1A). In the anodic scan, a shoulder (A1) at approximately −0.65 V and a peak (A2) approximately −0.5 V can be observed at both pHs; however, at lower pH, the second anodic peak is

more defined. At pH = 6, the anodic peak shifts towards higher potentials with decreasing phosphate concentration (Figure 1B). The total charge associated to the electrochemical process shows equal charge in both the anodic and cathodic scan of 52–60 $\mu C/cm^2$, which corresponds to ~0.2 electrons per surface atom. The charge values were found to be independent of the pH and phosphate concentration (Figure 1C,D).
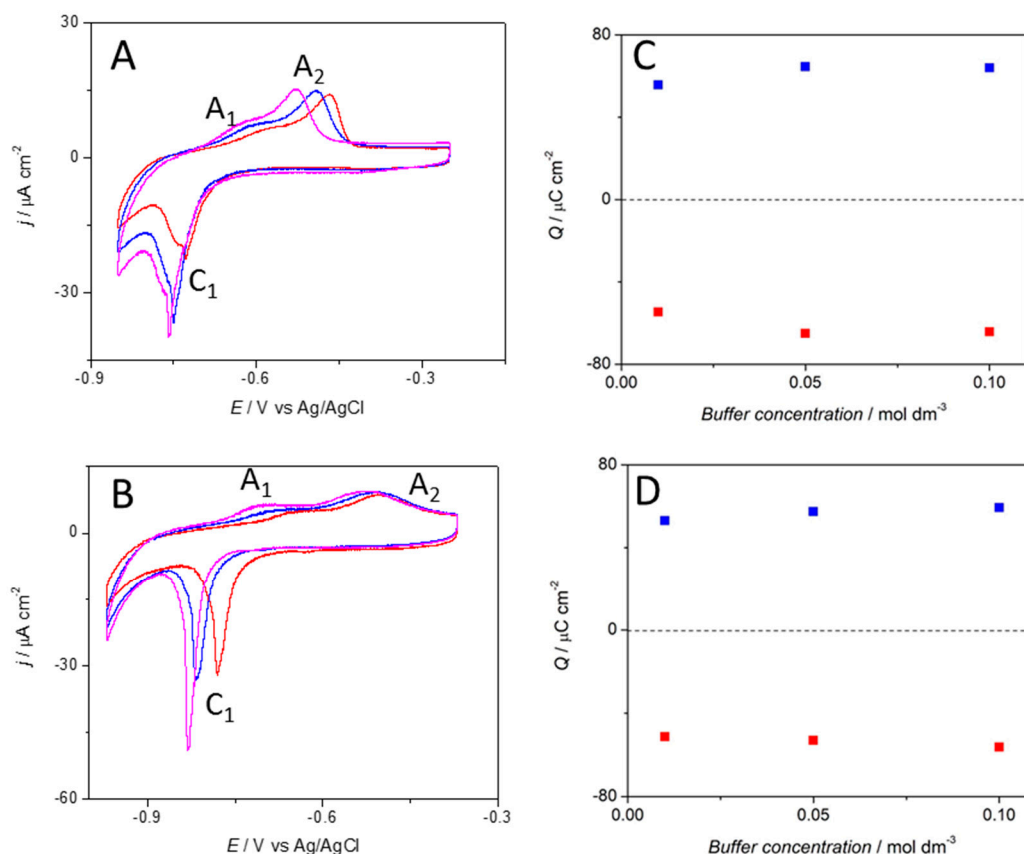

Figure 1. Cyclic voltammetry profiles of a Cu(111) electrode in a phosphate buffer solution at (**A**) pH = 6 and (**B**) pH = 8 with phosphate concentration equal to 0.01 M (red line), 0.05 M (blue line) and 0.1 M (magenta line). Scan rate ϑ= 0.02 V s^{-1}. (**C,D**) Charge involved in the oxidative (■) and reductive (■) process at the Cu(111) electrode as a function of the phosphate buffer concentration for pH = 6 and pH = 8 respectively.

3.2. Structural Characterization

The Cu(111) surface was investigated in phosphate buffer solution of concentration 0.1 M at pH = 8 with in-situ surface X-ray diffraction. Throughout the experiment, we noted the difference in the quality/morphology of the starting surface, which resulted specifically in a difference in reversibility of adsorption processes and stability. The differences in surface morphology are described in more detail below. Prior to any prolonged potential cycling resulting in excessive time spent at potentials where phosphate is adsorbed, all surfaces exhibited a rather similar change in structure as the potential was cycled. Figure 2 shows the X-ray intensities measured at the reciprocal space positions (0, 0, 1.4) and (0, 1, 0.5), shown as dotted and solid lines, respectively, and are representative of the potential dependent behaviour. The non-specular (0, 1, 0.5) position is sensitive to any changes in the atomic structure of the Cu(111) surface or to the adsorption of species into well-defined Cu adsorption sites, whereas the specular (0, 0, 1.4) position is sensitive to any changes in the surface normal electron density distribution including the electrolyte side of the interface. The results indicate that there is a

clear structural change at the interface, most likely involving restructuring of the Cu surface itself and this exhibits considerable hysteresis consistent with significant rearrangement of surface atoms.

Following the X-ray voltammetry (XRV) measurements, such as those shown in Figure 2, the Cu(111) surface structures were characterised while changing the potential in steps of 0.1 V over the range from −1.0 V to −0.5 V. For each potential, a rocking scan was measured at the (0, 1, 0.5) position and the integrated intensity obtained from this measurement is also shown in Figure 2 as black squares. It can be seen that these lie halfway in the hysteresis loop. The surface was characterised by detailed crystal truncation rod (CTR) measurements at potentials in the order −1.0 V, −0.9 V, −0.8 V, −0.7 V, −0.6 and −0.5 V, after which the potential was stepped back to −0.8 V to check the reproducibility and stability of the surface structure. The exact potential history of the experiment is shown in Figure 3 together with the integrated intensity and the peak width at the (0, 1, 0.5) position. It can be seen that the peak width did not change throughout the course of the experiment, indicating a stable surface, i.e., there was no change in surface morphology or domain size (which is inversely proportional to the width of the peak in the rocking scan). The integrated intensity changed with the applied potential as expected from the results shown in Figure 2. This change was reversible, as indicated by the two datasets recorded at −0.8 V, before and after the potential cycle, which gave the same structural parameters within the experimental error.
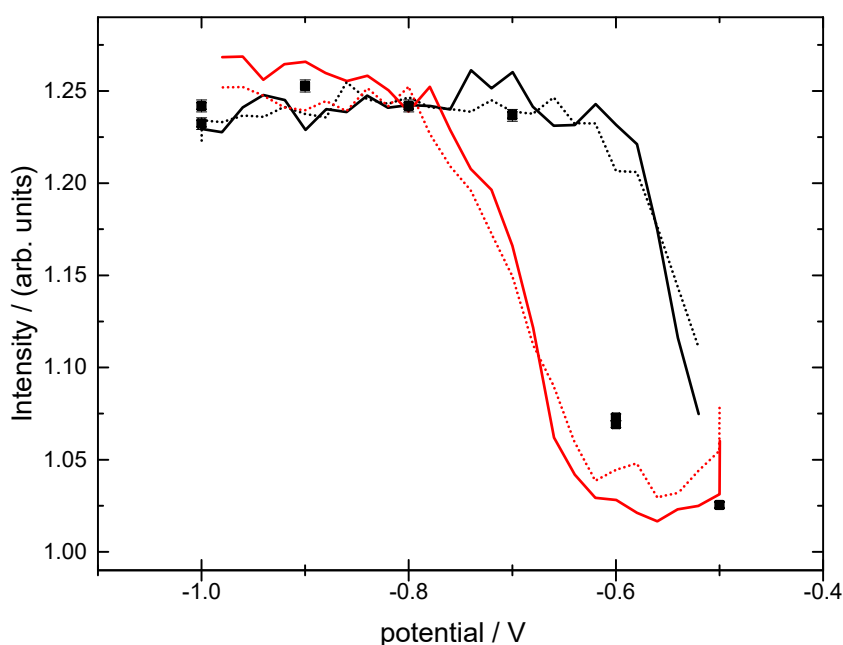

Figure 2. The potential dependence of the X-ray intensities measured at the non-specular, (0, 1, 0.5), (solid line) and specular, (0, 0, 1.4), anti-Bragg positions (sweep rate = 2 mV/s). In addition, the intensity obtained from measuring the integrated intensity at selected potentials under static conditions is also shown (black squares).

The CTR data and the best fit to the data obtained through a least-square fitting procedure for potentials of −0.5 V and −0.8 V are shown in Figure 4. The structural model used to fit the data allowed variation in the coverage of the topmost copper layer, the relaxation of the two topmost copper layers and also included a β-roughness factor which is typically used to model surface roughness in CTR measurements [22]. For the data measured at positive potentials it was also necessary to include an adsorbed oxygen layer with the oxygen atoms occupying *fcc/hcp* three-fold hollow Cu sites. The oxygen coverage and distance to the topmost Cu layer was allowed to vary to obtain the best fit. The obtained parameters for the best fits to the data at the different potentials are summarised in Figure 5. At potentials positive of −0.7 V, the coverage of the topmost copper layer started decreasing and

the oxygen coverage increased, together with an increased surface roughness. The inclusion of the oxygen layer in the structural model resulted in a decrease of the reduced $\chi2$ (indicating the goodness of fit in the least squares method) from 3.3 to 1.8 for the fit to the data recorded at -0.5 V. In-plane scans were measured at all potentials at L = 0.4 along the high symmetry <1, 0, L>, <0, 1, L> and <1, 1, L> directions but did not show any additional superstructure peaks. Thus, we conclude that there is no specific ordering of the phosphate or any oxygenated species into a commensurate ordered adsorbate or copper oxide layer, as such ordering would give rise to additional scattering features that would be detected in the scans along the high symmetry directions. Previous works, in gas phase and computational studies, suggest the formation of hexagonal or quasi-hexagonal structures on the Cu(111) surface upon oxygen adsorption, structures which can be viewed as the initial layer of a Cu_2O (111) film. The model proposed by Platzman et al. suggests a three-step oxidation mechanism comprising the formation of a Cu_2O layer, followed by the formation of a metastable overlayer of $Cu(OH)_2$ and finally the transformation of this metastable overlayer phase into CuO layer [23]. Our results in electrochemical environment do not show any of these ordered structures in the potential range under study.
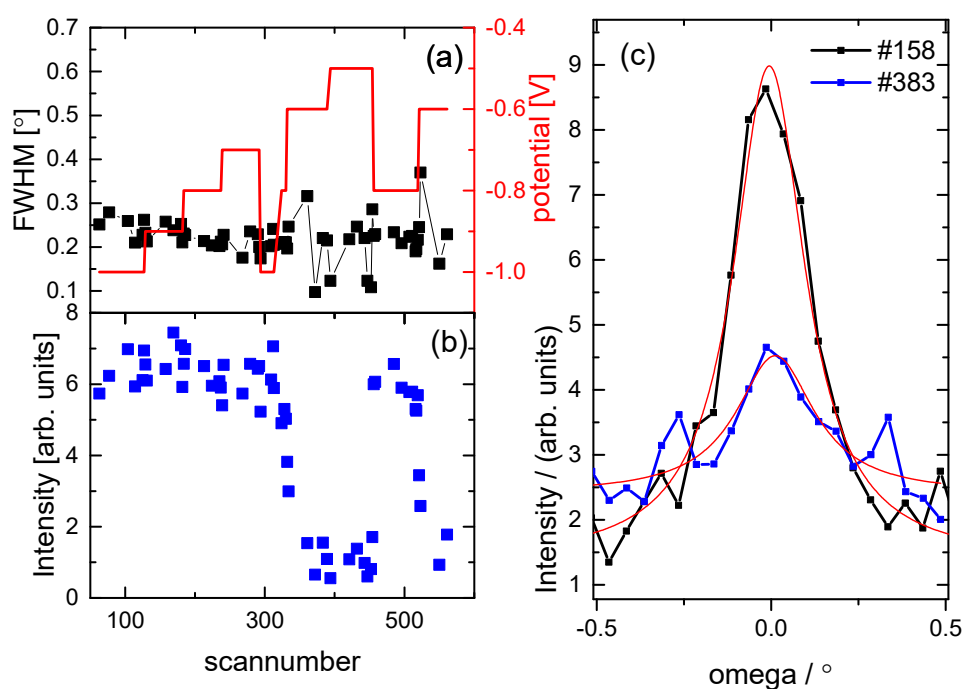

Figure 3. The surface stability has been monitored throughout the course of the experiment. (**a**) The full width half maximum (FWHM) and integrated intensity obtained from rocking scans at the (0, 1, 0.5) position are shown as function of the scan number during the experiment. The potential is also shown in red. The peak width is stable, indicating a stable surface with a domain size of ~100 nm. (**b**) The integrated intensity is changing reversibly with the applied potential. (**c**) The peak profiles of the rocking scan and the fit of the peak with a Lorentzian line shape are shown for scan numbers 158 and 383 at a potential of -0.9 V and -0.6 V, respectively.
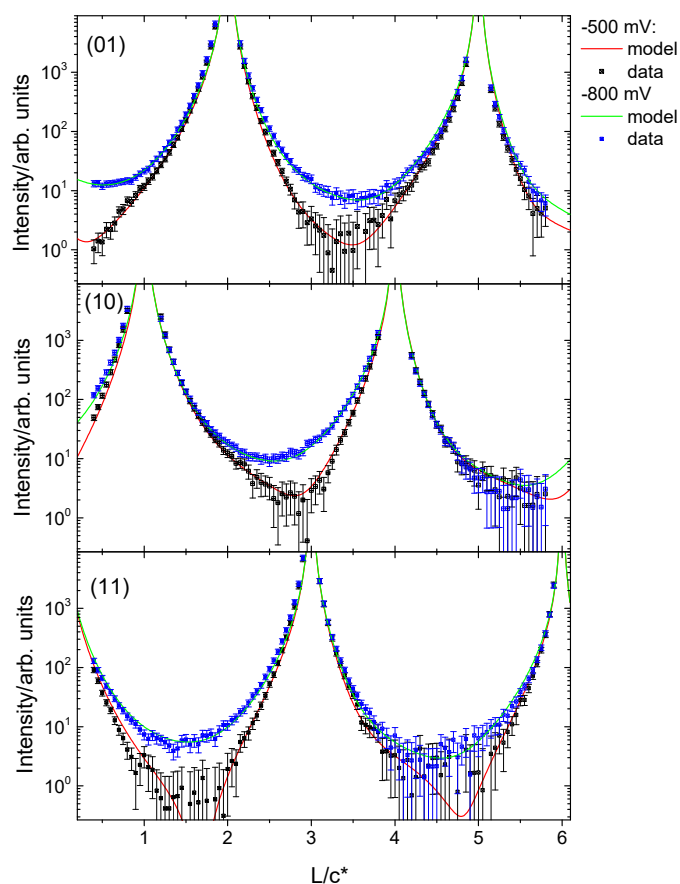
Figure 4. CTR data measured at −0.8 V (blue symbols) and −0.5 V (black symbols) together with the calculated fits to the data (solid lines) according to the structural model described in the text. At −0.5 V, an overall decrease in intensity at the surface sensitive positions can be observed. This has been modelled with an increased roughness and adsorption of an oxygenated species into the surface Cu layer. The change in intensity induced by the potential is fully reversible.

As noted above, the morphology of the surface depends crucially on the surface preparation and transfer into the electrochemical system. For the above case following the electropolishing of the Cu crystal, the transfer process to the X-ray electrochemical cell was smooth and the working electrode was contacted and held at −0.8 V as soon as the crystal was in the cell. Any exposure to oxygen during the preparation or not applying a potential in the oxygen reduction region immediately upon immersion into the cell resulted in a different surface morphology than for the surface described above. Previous work in gas phase has shown that at room temperature the oxidation of Cu(111) proceeds through the epitaxial growth of copper oxide islands [24,25]. It has been shown that, in gas phase, the growth of oxides on Cu(111) depends on the oxygen pressure and temperature and it can follows three possible processes: (i) growth from step edges; (ii) interrace growth from vacancy islands; and (iii) growth of on-terrace oxide [24,25]. The CTRs in this case showed additional peaks at (0, 1, 1), (0, 1, 4), (1, 0, 2) and (1, 0, 5) (Figure 6), which arose from stacking faults (twinning) induced by the nucleation of copper atoms into *hcp* sites. The CTR data in Figure 6 were best modelled by including additional Lorentzian peaks to represent the twinned Cu, rather than a smooth surface with stacking faults, and indicate that the peaks arose due to nano-crystalline copper islands on the surface. Due to the presence of the additional peaks resulting from the nano-crystalline copper at the surface, the CTRs could be reproduced reliably with a very simple model including surface roughness and Cu surface relaxation only, i.e., for this more complex surface, the fitting was not sensitive to the inclusion of an oxygen layer. The surface roughness and relaxation rely on the overall intensity change

across the whole range of *L* and the intensity distribution close to the Bragg peaks, respectively. We were not able to reliably include any coverage of individual atomic layers or oxygen atoms, which changed the intensity close to the anti-Bragg position as the intensity was dominated by the Lorentzian peaks arising from the nano-crystalline copper. Although these parameters, which are summarized in Figure 7, are only indicative, a similar trend in the potential dependent relaxation and roughness was observed when stepping the potential slowly positively. Surprisingly, at −0.8 V, modelling of the CTR data indicated a much lower surface roughness parameter, *β*, than the data shown in Figure 4. We attribute this to the presence of the nano-clustered copper islands acting as nucleation sites for copper ad-atoms, thus decreasing the overall surface roughness. The changes observed during the potential steps were, however, not reversible. Upon stepping back to the negative potential, an increase in the surface roughness, as indicated by the red symbols in Figure 7, could be observed. This increase in surface roughness was accompanied by a decrease in surface domain size and an increase in the size of the nano-crystalline copper domains present on the surface. This was shown by the rocking scan measurements at the (0, 1, 0.5) position (Figure 8), which, as for the data shown in Figure 3, also indicated the potential history of this sample. A gradual increase in the width of the rocking scan, from 0.2° to 0.4°, was observed, corresponding to a domain size decreasing from ~100 nm to ~50 nm. Correspondingly, the height D of the nano-clusters could be estimated from the width of the peaks observed in the CTR data in Figure 6, D = 2 π/ΔQ$_z$, and was found to grow in the course of the experiment from 20 to 40 nm. Thus, it can be concluded that this Cu surface—with Cu islands present on the surface—was unstable during potential cycling.
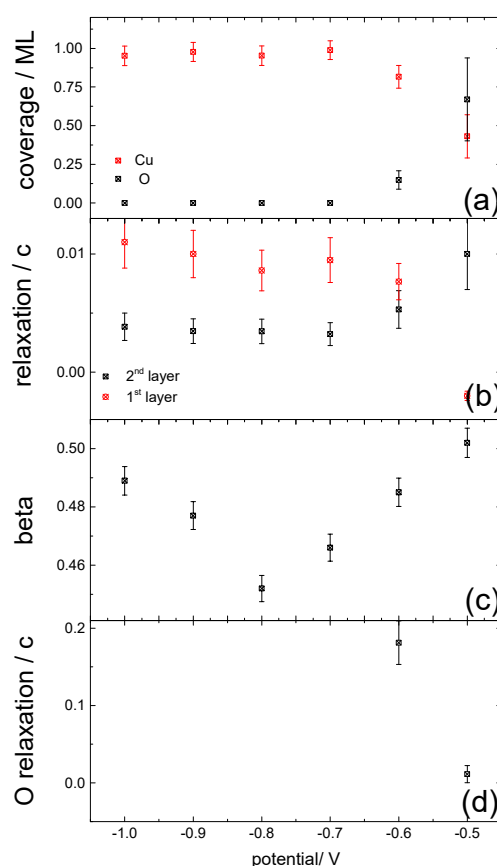

Figure 5. The structural parameters obtained from modelling the CTR data are plotted as a function of potential: (**a**) the coverage of the surface Cu layer and the adsorbed oxygen layer; (**b**) the relaxation of the top two copper layers; (**c**) the roughness as modelled through a β-roughness model; and (**d**) the Cu-O layer separation.
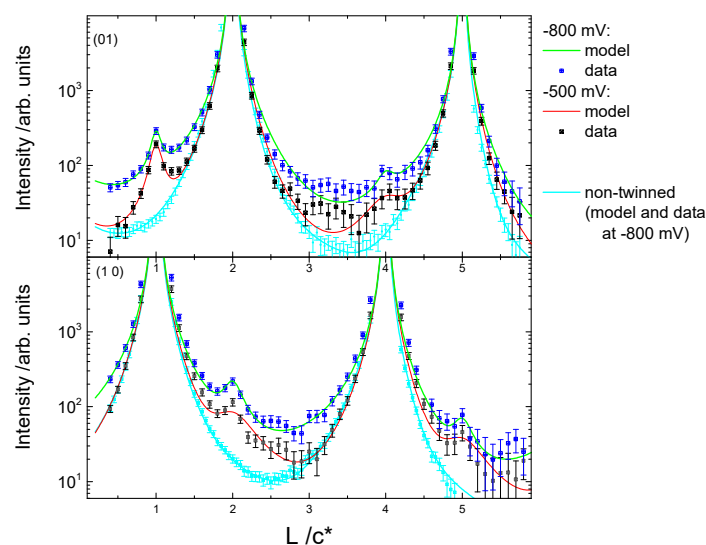
Figure 6. CTR data measured from a different Cu surface preparation at −0.8 V (blue symbols) and −0.5 V (black symbols) together with the calculated fits to the data (solid lines) according to the structural model described in the text. In comparison to the CTR data presented in Figure 4, additional peaks arising from Cu nano-islands can be observed.
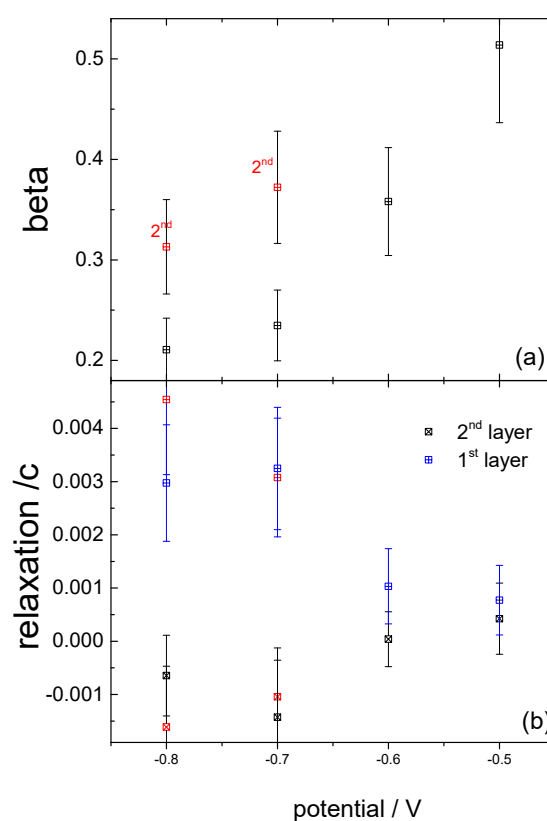

Figure 7. The structural parameters obtained from modelling the CTR data in Figure 6 are plotted as a function of potential: (**a**) the β-roughness factor; and (**b**) the relaxation of the two topmost atomic Cu layers. The data obtained after having stepped the potential to the positive limit are shown in red symbols. Although the potential-induced change in structure is similar, the roughness of the surface has increased.
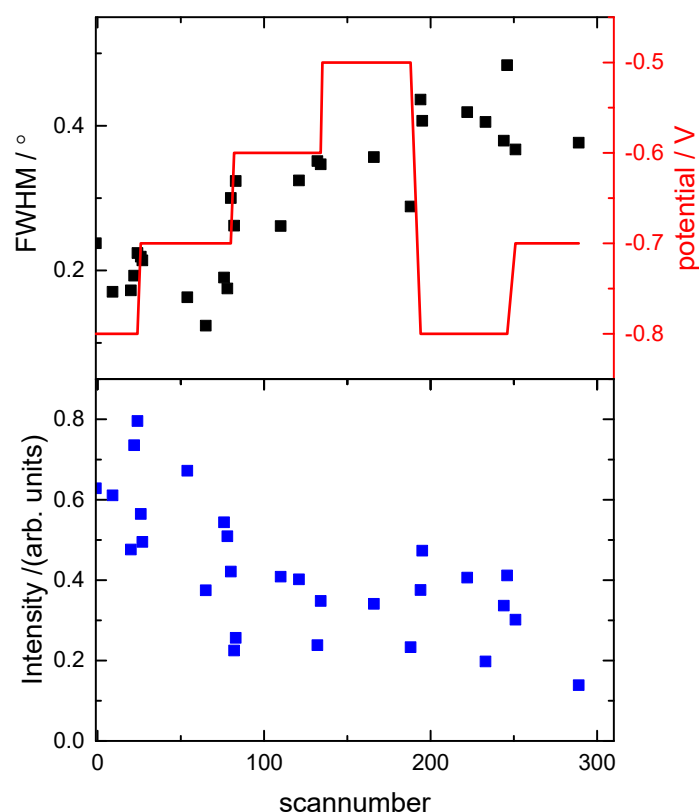
Figure 8. The surface stability of the Cu sample, which showed additional peaks arising from the presence of Cu nano-crystals, i.e., equivalent to the data shown in Figure 3: (a) the FWHM; and (b) the integrated intensity obtained from rocking scans at the (0, 1, 0.5) position as a function of the scan number during the experiment. The potential is also shown in red. The peak width is increasing and the integrated intensity is not recovering after having held the potential positively, indicating a change in surface morphology with increased roughness and smaller domain size during the course of the experiment.

4. Discussion

In this paper, we present a structural investigation of the Cu(111) electrode surface in phosphate-containing neutral electrolyte solution. We have found two different surface behaviours depending on the initial morphology and defect density of the surface observed directly after preparation and transfer into the X-ray electrochemical cell. In both cases, however, a clear structural transition with potential was found at −0.6 V, which coincides with a current peak in the anodic scan. The discussion of the structural results is based on the dataset presented in Figures 4–6, which gave the most concise insight into the underlying surface processes. At potentials negative of the observed transition, the coverage of the copper is constant and no potential dependent relaxation is observed. An increase in roughness can, however, be observed for increasingly cathodic potentials. The structural transition occurring at potentials >−0.7 V can be attributed to an increased surface roughness combined with adsorption of an oxygenated species, followed by the formation of a mixed copper-oxygen layer at positive potentials. This transition is accompanied by an inward relaxation of the surface Cu layer and a slight outward relaxation of the second atomic Cu layer.

Cyclic voltammograms were recorded at two different pH values and different phosphate concentrations to get an estimate of the charge transfer and possible coverage of an anionic layer and/or oxygenated species. For all electrolyte solutions, an anodic peak with a shoulder could be observed indicating a slow two-step adsorption process. The charge under the anodic and cathodic current peaks in the cyclic voltammetry corresponded to 0.2 electron transferred per surface atom. The

in situ X-ray structural analysis of the Cu(111) surface at -0.5 V gave an oxygen coverage $\theta_O = 0.6$. It is known that phosphate species have a tetrahedral structure with a P-O bond length of the order $d_{P-O} \sim 1.5\text{--}1.6$ Å, thus the corresponding O-O distance is $d_{O-O} \sim 2.44\text{--}2.62$ Å [26–28]. The atomic distance of the copper atoms at the Cu(111) surface is 2.556 Å, which is similar to the O-O distance in the phosphate, thus making the adsorption of phosphate or hydrogen phosphate with three oxygen atoms sitting in the same adsorption site likely. This suggests that the adsorbate species at -0.5 V can be either hydrogen phosphate or phosphate and not dihydrogen phosphate. The exact nature of the phosphate species and the adsorption process is, however, not fully understood. From the structural analysis at -0.6 V, it is clear that the difference between the data recorded at the two most positive potentials is not just due to a change in coverage of the adsorbed oxygenated species. The change in relaxation of the topmost copper layer and the change in the distance of the oxygen atoms to the Cu surface indicate an intermediate structure at this potential. This is also evident from the XRV and potentiostatic measurements presented in Figure 2.

To further elucidate the adsorption process, the peak positions in the cyclic voltammetry measured in 0.1 M phosphate solution at pH = 6 and pH = 8 are shown as a function of the logarithm of the scan rate in Figure 9. The cathodic peak and the first anodic peak (corresponding to the shoulder in the cyclic voltammogram) did not show a scan rate dependence, indicating a fast adsorption process, whereas the second anodic peaks showed a slope of approximately 0.12 V/log (scan rate/(V/s)), independent of the pH of the electrolyte, indicating is a slow process. The rate determining step in the adsorption process is thus associated with the second anodic peak. The surface X-ray diffraction data show that at the corresponding potentials a substantial rearrangement of the surface atomic structure took place. The X-ray voltammetry obtained in-situ shows a large hysteresis consistent with a slow mass transfer process. Static CTR measurement indicate the incorporation of oxygen/phosphate into the Cu surface resulting in mixed surface copper-oxide and increased surface roughness in this potential region. Structural rearrangements of the surface Cu layer with similarly slow kinetics have been observed in alkaline electrolytes [29,30]. In that case, the slow kinetics were associated with formation of a single Cu(I) oxide layer and a decrease of the Cu atomic density by 30% [31].
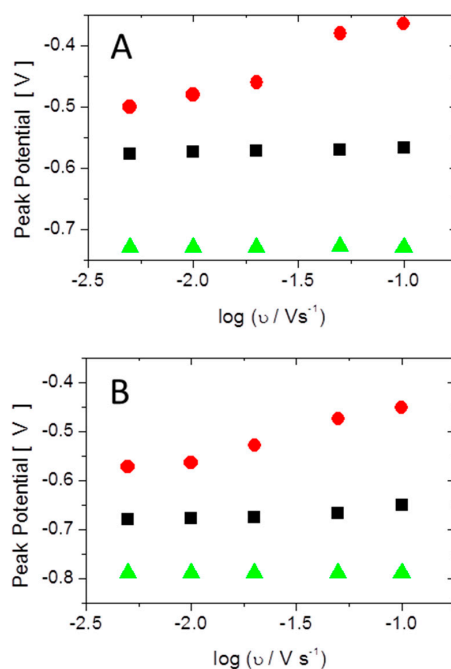

Figure 9. Peak potentials obtained from cyclic voltammograms are shown as function of the log of the scan rate: (**A**) pH = 6; and (**B**) pH = 8. The black and red symbols correspond to the first and second anodic peaks, respectively. The green symbols correspond to the cathodic peak.

With the acid dissociation constant pKa($H_2PO_4^-$/HPO_4^{2-}) = 7.2, at pH = 8 a proportion of 6% $H_2PO_4^-$ and 94% HPO_4^- is expected, thus mostly hydrogen phosphate. At pH = 6 a proportion of 87% $H_2PO_4^-$ and 13% HPO_4^{2-} is expected in the electrolyte solution. On gold and platinum surfaces, the adsorbed phosphate species has been found to be pH- and potential-dependent [32,33]. In contrast, on copper surfaces, phosphate dihydrogen was found to adsorb for acidic electrolyte solutions (pH < 5) but not in alkaline solution (pH > 9) [34]. Although we cannot totally exclude that dihydrogen is adsorbing in the first step on the Cu surface, the fact that the two adsorption steps were observed at pH = 6 and pH = 8 in the electrochemical data and did not show a difference in the kinetics of the processes, suggest that the adsorption process occurred through a similar mechanism. In addition, a more covalent bonding between the oxygen of the phosphate and copper was found, in comparison to silver and gold [34], and this could lead to the atomic rearrangement and slow mass transport observed in the X-ray measurements.

By combining the structural and electrochemical results, we propose the following adsorption mechanism: The first peak observed in the cyclic voltammograms corresponds to adsorption of hydrogen phosphate to the surface (either directly or through the deprotonation of dihydrogen phosphate depending on the pH). This is supported by the structural data where a small amount of oxygen was found to be specifically adsorbed into three-fold hollow sites on the Cu surface. The second anodic peak is associated with the deprotonation of the hydrogen phosphate and the adsorption of the phosphate anion which forms a strong bond with the Cu surface leading to an atomic rearrangement involving the incorporation of three oxygen atoms from the phosphate into the surface Cu layer. This process is totally reversible, as also confirmed by the electrochemical characterization which gives the same charge under the peak in the cyclic voltammogram for the anodic and cathodic process.

The elucidation of the adsorption process helps in understanding the differences in stability of the Cu(111) electrodes during adsorption process and the dependence on the details of Cu surface preparation. The in-situ X-ray diffraction data enable three main properties of the surface contributing to the morphology to be distinguished: (a) the domain size of the atomic terraces present at the surface; (b) the presence of Cu nano-crystals at the surface; and (c) the overall atomic roughness, described through the β-model and hereafter referred to as rugosity. We have shown that, even though the Cu(111) surfaces exhibit identical terrace lengths, the rugosity of the surface at terrace level might be different. The Cu(111) surface with large rugosity shows a reversible adsorption process of phosphates and oxygen incorporation into the crystalline structure. On the other hand, the Cu(111) surface with copper nano-crystals present on the surface showed degradation upon phosphate adsorption/desorption driven by the potential cycling. Surprisingly the rugosity was larger on the surface showing reversible adsorption, the reversible nature of the adsorption/desorption being evident from the stable intensity at the anti-Bragg position of the CTRs. The oxygen induced reconstruction of the Cu(111) surface at room temperature have shown the formation of a disordered surface overlayer, with O and Cu atoms at different heights [35]. It has been proposed that the formation of this disorder overlayer favours the oxygen diffusion on Cu (111) leading to fast nucleation of a large number of oxide islands. We propose a similar process in electrochemical media through the oxygens of the adsorbed phosphates.

As the adsorption of phosphate increases the rugosity of the surface, we associate the differences in stability of the two surfaces to the presence of surface defects acting as nucleation sites for Cu ad-atoms created during the phosphate incorporation into the surface Cu layer. Depending on the surface morphology, these atoms can be incorporated into the nano-crystals present on the surface, thus leading to further roughening and decrease in the surface domain size, i.e., the Cu surface is unstable. On a Cu electrode surface with high rugosity, no single nucleation sites stand out and the formation of nano-crystals is prevented. This is a more stable Cu electrode surface exhibiting a reversible phosphate adsorption process.

5. Conclusions

In this paper, we present electrochemical and in-situ surface X-ray diffraction measurements of phosphate adsorption onto Cu(111) electrodes. The underlying mechanism of the phosphate adsorption and deprotonation of the (di)-hydrogen phosphate was accompanied by a roughening of the Cu surface. We report for the first time the roughening of the Cu surface through the formation of a mixed copper–oxygen layer, where the oxygen from an adsorbed phosphate species was incorporated into the surface Cu layer. The stability of the Cu(111) surface and the change of rugosity upon potential cycling strongly depend on the preparation method and history of the electrode. It was shown that the presence of Cu islands on the Cu(111) surface leads to a 3D nucleation and growth mechanism which causes irreversible changes in surface morphology. The results demonstrate the importance of controlling the surface preparation of copper catalysts, as this determines the stability of the catalyst under operation conditions for the electrochemical CO_2 reduction reaction. The incorporation of oxygen into the metal surface from the adsorbed phosphate anion is a process that could also be relevant to the study of similar oxoanions, such as sulphate, and their role in the stability of electrocatalysts during oxidation processes.

References

1. Larrazábal, G.O.; Martín, A.J.; Pérez-Ramírez, J. Building blocks for high performance in electrocatalytic CO_2 reduction: materials, optimization strategies, and device engineering. *J. Phys. Chem. Lett.* **2017**, *8*, 3933–3944.
2. Arán-Ais, R.M.; Gao, D.; Roldan cuenya, B. structure- and electrolyte-sensitivity in CO_2 electroreduction. *Acc. Chem. Res.* **2018**, *51*, 2906–2917. [CrossRef] [PubMed]
3. Engstfeld, A.K.; Maagaard, T.; Horch, S.; Chorkendorff, I.; Stephens, I.E.L. Polycrystalline and Single-Crystal Cu Electrodes: Influence of Experimental Conditions on the Electrochemical Properties in Alkaline Media. *Chem. A Eur. J.* **2018**, *24*, 17743–17755. [CrossRef] [PubMed]
4. Grosse, P.; Gao, D.; Scholten, F.; Sinev, I.; Mistry, H.; Roldan Cuenya, B. Dynamic Changes in the Structure, Chemical State and Catalytic Selectivity of Cu Nanocubes during CO_2 Electroreduction: Size and Support Effects. *Angew. Chem.* **2018**, *130*, 6300–6305. [CrossRef]
5. Mistry, H.; Varela, A.S.; Bonifacio, C.S.; Zegkinoglou, I.; Sinev, I.; Choi, Y.-W.; Kisslinger, K.; Stach, E.A.; Yang, J.C.; Strasser, P.; et al. Highly selective plasma-activated copper catalysts for carbon dioxide reduction to ethylene. *Nat. Commun.* **2016**, *7*, 12123. [CrossRef] [PubMed]
6. Resasco, J.; Chen, L.D.; Clark, E.; Tsai, C.; Hahn, C.; Jaramillo, T.F.; Chan, K.; Bell, A.T. Promoter Effects of Alkali Metal Cations on the Electrochemical Reduction of Carbon Dioxide. *J. Am. Chem. Soc.* **2017**, *139*, 11277–11287. [CrossRef] [PubMed]
7. Le Duff, C.S.; Lawrence, M.J.; Rodriguez, P. Role of the Adsorbed Oxygen Species in the Selective Electrochemical Reduction of CO2 to Alcohols and Carbonyls on Copper Electrodes. *Angew. Chem. Int. Ed.* **2017**, *56*, 12919–12924. [CrossRef] [PubMed]

8. Kas, R.; Kortlever, R.; Milbrat, A.; Koper, M.T.M.; Mul, G.; Baltrusaitis, J. Electrochemical CO_2 reduction on Cu_2 O-derived copper nanoparticles: controlling the catalytic selectivity of hydrocarbons. *Phys. Chem. Chem. Phys.* **2014**, *16*, 12194–12201. [CrossRef] [PubMed]

9. Mandal, L.; Yang, K.R.; Motapothula, M.R.; Ren, D.; Lobaccaro, P.; Patra, A.; Sherburne, M.; Batista, V.S.; Yeo, B.S.; Ager, J.W.; et al. Investigating the Role of Copper Oxide in Electrochemical CO_2 Reduction in Real Time. *ACS Appl. Mater. Interfaces* **2018**, *10*, 8574–8584. [CrossRef] [PubMed]

10. Verdaguer-Casadevall, A.; Li, C.W.; Johansson, T.P.; Scott, S.B.; McKeown, J.T.; Kumar, M.; Stephens, I.E.L.; Kanan, M.W.; Chorkendorff, I. Probing the Active Surface Sites for CO Reduction on Oxide-Derived Copper Electrocatalysts. *J. Am. Chem. Soc.* **2015**, *137*, 9808–9811. [CrossRef] [PubMed]

11. Lee, S.; Kim, D.; Lee, J. Electrocatalytic Production of C3-C4 Compounds by Conversion of CO_2 on a Chloride-Induced Bi-Phasic Cu_2 O-Cu Catalyst. *Angew. Chem. Int. Ed.* **2015**, *54*, 14701–14705. [CrossRef] [PubMed]

12. Eilert, A.; Cavalca, F.; Roberts, F.S.; Osterwalder, J.; Liu, C.; Favaro, M.; Crumlin, E.J.; Ogasawara, H.; Friebel, D.; Pettersson, L.G.M.; et al. Subsurface Oxygen in Oxide-Derived Copper Electrocatalysts for Carbon Dioxide Reduction. *J. Phys. Chem. Lett.* **2017**, *8*, 285–290. [CrossRef] [PubMed]

13. Friebel, D.; Broekmann, P.; Wandelt, K. Electrochemical in situ STM study of a Cu(111) electrode in neutral sulfate containing electrolyte. *Phys. Status Solidi* **2004**, *201*, 861–869. [CrossRef]

14. Lucas, C.A.; Markovic, N.M. Structure Relationships in Electrochemical Reactions. In *Encyclopedia of Electrochemistry*; Wiley-VCH Verlag GmbH & Co. KGaA: Weinheim, Germany, 2007; ISBN 9783527610426.

15. Gründer, Y.; Lucas, C.A. Surface X-ray diffraction studies of single crystal electrocatalysts. *Nano Energy* **2016**, *29*, 378–393. [CrossRef]

16. Lucas, C.A.; Thompson, P.; Gründer, Y.; Markovic, N.M. The structure of the electrochemical double layer: Ag(111) in alkaline electrolyte. *Electrochem. Commun.* **2011**, *13*, 1205–1208. [CrossRef]

17. Sisson, N.; Gründer, Y.; Lucas, C.A. Structure and Stability of Underpotentially Deposited Ag on Au(111) in Alkaline Electrolyte. *J. Phys. Chem. C* **2016**, *120*, 16100–16109. [CrossRef]

18. Nicklin, C.; Arnold, T.; Rawle, J.; Warne, A. Diamond beamline I07: A beamline for surface and interface diffraction. *J. Synchrotron Radiat.* **2016**, *23*, 1245–1253. [CrossRef] [PubMed]

19. Vlieg, E. A (2 + 3)-Type Surface Diffractometer: Mergence of the z-Axis and (2 + 2)-Type Geometries. *J. Appl. Crystallogr.* **1998**, *31*, 198–203. [CrossRef]

20. Schlepütz, C.M.; Herger, R.; Willmott, P.R.; Patterson, B.D.; Bunk, O.; Brönnimann, C.; Henrich, B.; Hülsen, G.; Eikenberry, E.F. Improved data acquisition in grazing-incidence X-ray scattering experiments using a pixel detector. *Acta Crystallogr. Sect. A Found. Crystallogr.* **2005**, *61*, 418–425. [CrossRef] [PubMed]

21. Schlepütz, C.M.; Mariager, S.O.; Pauli, S.A.; Feidenhansl, R.; Willmott, P.R. Angle calculations for a (2+3)-type diffractometer: Focus on area detectors. *J. Appl. Crystallogr.* **2011**, *44*, 73–83. [CrossRef]

22. Robinson, I.K. Crystal truncation rods and surface roughness. *Phys. Rev. B* **1986**, *33*, 3830–3836. [CrossRef]

23. Platzman, I.; Brener, R.; Haick, H.; Tannenbaum, R. Oxidation of Polycrystalline Copper Thin Films at Ambient Conditions. *J. Phys. Chem. C* **2008**, *112*, 1101–1108. [CrossRef]

24. Pérez León, C.; Sürgers, C.; Löhneysen, H. Formation of copper oxide surface structures via pulse injection of air onto Cu(111) surfaces. *Phys. Rev. B* **2012**, *85*, 035434.

25. Matsumoto, T.; Bennett, R.A.; Stone, P.; Yamada, T.; Domen, K.; Bowker, M. Scanning tunneling microscopy studies of oxygen adsorption on Cu(1 1 1). *Surf. Sci.* **2001**, *471*, 225–245. [CrossRef]

26. Gamoke, B.; Neff, D.; Simons, J. Nature of PO Bonds in Phosphates. *J. Phys. Chem. A* **2009**, *113*, 5677–5684. [CrossRef] [PubMed]

27. Pye, C.C.; Rudolph, W.W. An ab Initio, Infrared, and Raman Investigation of Phosphate Ion Hydration. *J. Phys. Chem. A* **2003**, *107*, 8746–8755. [CrossRef]

28. Rose, J.; Flank, A.M.; Masion, A.; Bottero, J.Y.; Elmerich, P. Nucleation and Growth Mechanisms of Fe Oxyhydroxide in the Presence of PO4 Ions. 2. P K-Edge EXAFS Study. *Langmuir* **1997**, *13*, 1827–1834. [CrossRef]

29. Maurice, V.; Strehblow, H.H.; Marcus, P. In situ STM study of the initial stages of oxidation of Cu(111) in aqueous solution. *Surf. Sci.* **2000**, *458*, 185–194. [CrossRef]

30. Kunze, J.; Maurice, V.; Klein, L.H.; Strehblow, H.H.; Marcus, P. In situ scanning tunneling microscopy study of the anodic oxidation of Cu(111) in 0.1 M NaOH. *J. Phys. Chem. B* **2001**, *105*, 4263–4269. [CrossRef]

31. Kunze, J.; Maurice, V.; Klein, L.H.; Strehblow, H.-H.; Marcus, P. In situ STM study of the anodic oxidation of Cu(0 0 1) in 0.1 M NaOH. *J. Electroanal. Chem.* **2003**, *554–555*, 113–125. [CrossRef]

32. Yaguchi, M.; Uchida, T.; Motobayashi, K.; Osawa, M. Speciation of Adsorbed Phosphate at Gold Electrodes: A Combined Surface-Enhanced Infrared Absorption Spectroscopy and DFT Study. *J. Phys. Chem. Lett.* **2016**, *7*, 3097–3102. [CrossRef] [PubMed]

33. Gisbert, R.; García, G.; Koper, M.T.M. Adsorption of phosphate species on poly-oriented Pt and Pt(1 1 1) electrodes over a wide range of pH. *Electrochim. Acta* **2010**, *55*, 7961–7968. [CrossRef]

34. Niaura, G.; Gaigalas, A.K.; Vilker, V.L. Surface-Enhanced Raman Spectroscopy of Phosphate Anions: Adsorption on Silver, Gold, and Copper Electrodes. *J. Phys. Chem. B* **1997**, *101*, 9250–9262. [CrossRef]

35. Jensen, F.; Besenbacher, F.; Lægsgaard, E.; Stensgaard, I. Oxidation of Cu(111): two new oxygen induced reconstructions. *Surf. Sci. Lett.* **1991**, *259*, L774–L780.